Digital Image Watermarking Using Balanced Multiwavelets

Lahouari Ghouti, *Member, IEEE*, Ahmed Bouridane, *Member, IEEE*, Mohammad K. Ibrahim, *Senior Member, IEEE*, and Said Boussakta, *Senior Member, IEEE*

***Abstract*—In this paper, a robust watermarking algorithm using balanced multiwavelet transform is proposed. The latter transform achieves simultaneous orthogonality and symmetry without requiring any input prefiltering. Therefore, considerable reduction in computational complexity is possible, making this transform a good candidate for real-time watermarking implementations such as audio broadcast monitoring and DVD video watermarking. The embedding scheme is image adaptive using a modified version of a well-established perceptual model. Therefore, the strength of the embedded watermark is controlled according to the local properties of the host image. This has been achieved by the proposed perceptual model, which is only dependent on the image activity and is not dependent on the multifilter sets used, unlike those developed for scalar wavelets. This adaptivity is a key factor for achieving the imperceptibility requirement often encountered in watermarking applications. In addition, the watermark embedding scheme is based on the principles of spread-spectrum communications to achieve higher watermark robustness. The optimal bounds for the embedding capacity are derived using a statistical model for balanced multiwavelet coefficients of the host image. The statistical model is based on a generalized Gaussian distribution. Limits of data hiding capacity clearly show that balanced multiwavelets provide higher watermarking rates. This increase could also be exploited as a side channel for embedding watermark synchronization recovery data. Finally, the analytical expressions are contrasted with experimental results where the robustness of the proposed watermarking system is evaluated against standard watermarking attacks.**

***Index Terms*—Balanced multiwavelets, data hiding, embedding capacity, game theory, image watermarking, information theory, scalar wavelets.**

I. INTRODUCTION

WITH the rapid growth and widespread use of network distributions of digital media content, there is an urgent need for protecting the copyright of digital content against piracy and malicious manipulation. Watermarking systems have been proposed as a possible and efficient answer to these concerns. While most of the available research papers have focused on developing new paradigms for watermark embedding, the watermarking community recently recognized the need to develop a guiding theory to describe the fundamental limits of available and yet-to-develop watermarking systems. Therefore, information-theoretic watermarking research began to emerge [1]–[4]. In particular, a theory has recently been developed to establish the fundamental limits of the watermarking (data-hiding) problem. Around the same time, Cox *et al.* [5] have also recognized that one may view watermarking as communications with side information known at the encoder. This is reminiscent of the communications problem with a fixed noisy channel and side information at the encoder [6]. Interestingly enough, Chen and Wornell [7] were the first to establish the analogy between watermarking and communications with side information problems. They proposed an embedding strategy where the design of the watermarking codes takes into the consideration the availability of the side information at the encoder side. Their scheme, quantization index modulation (QIM), may be viewed as a specific Costa scheme [8].

The goal of this paper is twofold: 1) to develop a novel image-adaptive watermarking scheme using balanced multiwavelets and 2) to derive the watermarking (data-hiding) capacity of the proposed scheme using various statistical models for the host image. The watermark embedding is governed by an efficient, yet simple, perceptual model based on a subband decomposition that has been specifically adopted to the balanced multiwavelet transform used in this paper. The proposed watermarking system is described in Section II where the motivations behind the use of balanced multiwavelets and subband just-noticeable difference (JND) profile are outlined. Section III describes the basic mathematical model for the image watermarking problem. Relevant models for attack channels are reviewed therein. Then, we will derive the data-hiding capacity of the proposed scheme for the considered channel models. The performance of the watermarking system is evaluated in Section IV, where its robustness against benchmark attacks is assessed. Finally, the conclusion is presented in Section V.

II. PROPOSED WATERMARKING SYSTEM

As mentioned in the previous section, watermarking can be looked at as a problem of communications through a noisy channel.[1] As a means to combatting this noise or interference, spread-spectrum techniques are employed to allow

Manuscript received July 1, 2004; revised May 10, 2005. The associate editor coordinating the review of this manuscript and approving it for publication was Dr. Ton Kalker.

L. Ghouti and A. Bouridane are with the School of Computer Science, Queen's University of Belfast, Belfast BT7 1NN, U.K. (e-mail: L.Ghouti@qub.ac.uk; A.Bouridane@qub.ac.uk).

M. K. Ibrahim is with the School of Engineering and Technology, De Montfort University, Leicester LE1 9BH, U.K. (e-mail: ibrahim@dmu.ac.uk).

S. Boussakta is with the School of Electronic and Electrical Engineering, The University of Leeds, Leeds LS2 9TJ, U.K. (e-mail: S.Boussakta@leeds.ac.uk).

Digital Object Identifier 10.1109/TSP.2006.870624

---

[1] According to [7], watermarking systems can be divided into two broad classes: 1) host-interference nonrejecting schemes and 2) host-interference rejecting schemes. In the former, the host signal is considered as a source of interference at the decoder unlike in the latter class.

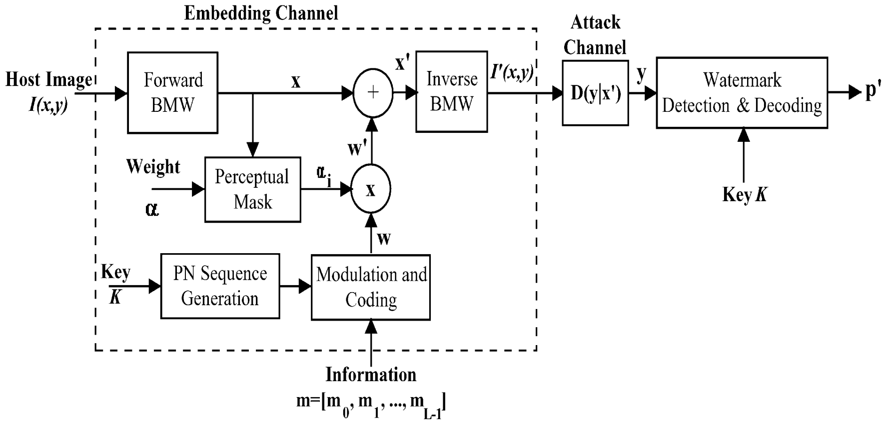

Fig. 1. Proposed public spread-spectrum watermarking system.

reliable communication in such noisy environments. In this case, the watermark data is coded with a pseudorandom code sequence to spread the power spectrum of the information data; thus, increasing its robustness against noise. In the proposed watermarking system, we will use the direct sequence spread-spectrum approach. First, we give an outline of the *public* watermarking model and assumptions. Then, we will describe the watermark embedding algorithm. To allow an adaptive embedding, the proposed watermarking system analyzes the host image activity using a perceptual model based on a well-established subband paradigm [9]. However, because the perceptual model was initially developed to derive the JND profile for a subband image coder, we will outline the necessary modifications to integrate this model with balanced multiwavelets. Watermark detection stage is then outlined.

A. Watermarking System Model

A generic model of the proposed watermarking system is shown in Fig. 1. The information data $\mathbf{m}$ is an L-bit binary sequence which modulates some pseudorandom sequences. The process of watermark encoding is independent of the host image $I(x, y)$. However, it is worth noting that weighting the watermark with a visual mask derived from the host image does not violate this independence. The watermark is modulated by the information data and is simply added to the host image. The latter, in this case, is viewed as additive noise with respect to the watermark. The watermarked image $I^{'}(x, y)$ will be transmitted through a possibly noisy channel, having a model of its own, and the received corrupted image $\mathbf{y}(x, y)$ will be processed by the watermark detector/decoder stage. Prior to watermark embedding, the host image is projected in a transform domain using the balanced multiwavelet transform [10]. The merits of this transform will be reviewed later in this paper. The effects incurred to the watermarked channel by the transmission channel and most of the possible intentional and accidental attacks can be modeled using emerging attack models [2], [4]. Elegant information-theoretic insights can be gained using these attack models where even the more challenging class of geometric attacks can be taken into consideration.[2]

B. Watermark Embedding Algorithm

The main steps performed in the proposed watermarking system are summarized below.

1) A binary pseudorandom image consisting of ± 1 is generated using the *private* embedding key K.
2) Compute the forward-balanced multiwavelet (BMW) transform of the host signal ($I(x, y)$ in our case) to get the subband coefficients x_i.
3) Estimate the perceptual weights α_i using the modified JND profile of Chou's model for each transform subband *independently*.
4) Modulate the pseudorandom sequence by the watermark information data $\mathbf{m}$ to get the spread-spectrum modulated watermark sequence w.
5) Scale the modulated watermark signal with the perceptual weights (α_i) estimated in Step 3.
6) Perform watermark embedding using the following additive-multiplicative rule: $x_i^{'} = x_i(1 + \alpha_i w_i)$.
7) Finally, the watermarked image $I^{'}(x, y)$ is obtained by performing the inverse BMW transform of the watermarked coefficients $x_i^{'}$.

Following the notation used for the derivation of data-hiding capacity in Section III, the watermark embedding rule is restated as follows[3]:

$$x_j = s_j(1 + \alpha_j pn_j m_k), \quad j = 1, 2 \ldots, \chi \tag{1}$$

where

s_j	the host transform coefficient selected from a set to hide the watermark bit m_k; each watermark bit $m_k, 1 \leq k \leq M$ is embedded in a set containing χ host transform coefficients; $m_k \pm 1$;
x_j	watermarked transform coefficient;
α_j	JND profile weight calculated based on the perceptual model described in Section II-B-2); α_j represents the variable and changes across subbands and decomposition levels as shown in Section II-B-2);
pn_j	pseudorandom coefficient used to modulate the watermark bit m_k.

---

[2] In fact, Moulin and Mihçak [2] model geometric attacks as a global warping operation that takes a specific form.

[3] This formulation encompasses the inclusion of error-coding through simple repetition-coding, block coding, or convolutional coding.

It is worth mentioning that the novelty of the proposed watermarking system lies in 1) the use of balanced multiwavelet transform, 2) the image-adaptive watermark embedding using a new perceptual model derived from a conventional subband JND profile, and 3) the improved data-hiding capacity due to the inherent structure of the transform subbands. Because the balanced multiwavelet transform is a relatively new multiresolution analysis (MRA) tool, we devote to it an independent subsection to highlight its mathematical details and merits.

1) Multiwavelets and Balanced Multiwavelets: Orthogonality is a desirable property for software/hardware implementation, while symmetry provides comfort to image perception [11]. In the context of image coding applications, the following three properties are important: 1) orthogonality to ensure the decorrelation of subband coefficients, 2) symmetry (i.e., linear phase) to process finite length signals without redundancy and artifacts, and 3) finite-length filters for computational efficiency. However, most real scalar wavelet transforms fail to possess these properties simultaneously. To circumvent these limitations, multiwavelets have been proposed where orthogonality and symmetry are allowed to co-exist by relaxing the time-invariance constraint [10].

a) Multiwavelets: Multiwavelets may be considered as generalization of scalar wavelets. However, some important differences exist between these two types of multiresolution transforms. In particular, whereas scalar wavelets have a single scaling $\phi(t)$ and wavelet function $\psi(t)$, multiwavelets may have two or more scaling and wavelet functions. In general, r scaling functions can be written using the vector notation $\Phi(t) = [\phi_1(t)\phi_2(t)\cdots\phi_r(t)]^T$, where $\Phi(t)$ is called the *multiscaling* function. In the same way, we can define the *multiwavelet* function using r wavelet functions as $\Psi(t) = [\psi_1(t)\psi_2(t)\cdots\psi_r(t)]^T$. The scalar case is represented by $r = 1$. Most of developed multiwavelet transforms use two scaling and wavelet functions, while r can take, theoretically, any value. Similar to scalar wavelets, for $r = 2$, the multiscaling function satisfies the following two-scale equation:

$$\Phi(t) = \sqrt{2}\sum_{k=-\infty}^{\infty} H_k \Phi(2t-k) \tag{2}$$

$$\Psi(t) = \sqrt{2}\sum_{k=-\infty}^{\infty} G_k \Phi(2t-k). \tag{3}$$

However, it should be noted that $\{H_k\}$ and $\{G_k\}$ are 2×2 matrix filters defined as

$$H_k = \begin{bmatrix} h_0(2k) & h_0(2k+1) \\ h_1(2k) & h_1(2k+1) \end{bmatrix} \tag{4}$$

$$G_k = \begin{bmatrix} g_0(2k) & g_0(2k+1) \\ g_1(2k) & g_1(2k+1) \end{bmatrix} \tag{5}$$

where $\{h_k(n)\}$ and $\{g_k(n)\}$ are the scaling and wavelet filter sequences such that $\sum_n h_k^2(n) = 1$ and $\sum_n g_k^2(n) = 1$ for $k = 1, 2$.

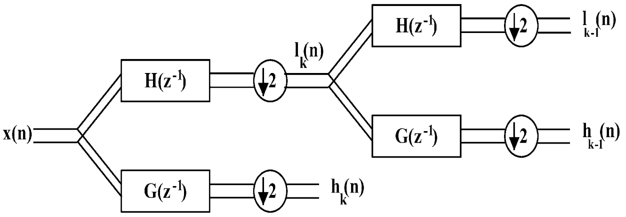

Fig. 2. Multiwavelet filter bank using one iteration.

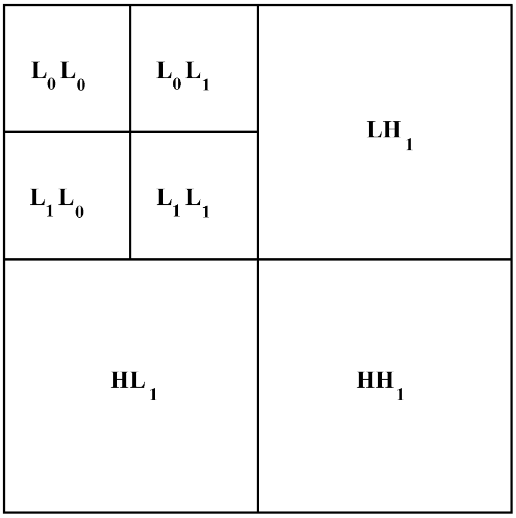

Fig. 3. Multiwavelet subbands using single-level decomposition.

The matrix elements in the filters, given by (4) and (5), provide more degrees of freedom than a traditional scalar wavelet. Due to these extra degrees of freedom, multiwavelets can simultaneously achieve orthogonality, symmetry, and high order of approximation. However, the multichannel nature of multiwavelets yields a subband structure that is different from that using scalar wavelets [12].

Fig. 2 clearly shows that multiwavelets are defined for one-dimensional (1-D) and two-dimensional (2-D) vector-valued signals. Using multiwavelets, the resulting approximation subband has a structure similar to that shown in Fig. 3.

The structure of the approximation subband does not obey the structure on which most successful embedded coders, such as set partitioning in hierarchical trees (SPIHT) algorithm, are designed. Like image coders, watermarking systems have to deal with the major hurdle of handling the approximation sub-blocks differently. In Fig. 3, these sub-blocks are denoted by L_0L_0, L_0L_1, L_1L_0, and L_1L_1, respectively. Usually only the sub-block L_0L_0 represents an approximation of the original image [12]. The differing spectral characteristics of these sub-blocks constitute a major problem for systems based on multiwavelets. Fig. 4 shows these sub-blocks and their spectral contents for Lena image.

To obtain a structure similar to that of the approximation subband in scalar wavelets, the multiwavelet coefficients in the approximation sub-blocks are combined using the shuffling technique proposed by Martin and Bell [12]. However, for unbalanced multiwavelets, this combination does not yield a correct approximation of the input image as shown in Fig. 5.

b) Balanced Multiwavelets: Lebrun and Vetterli [10] indicate that the balancing order of the multiwavelet is indicative of its energy compaction efficiency. However, a high balancing order alone does not ensure good image compression performance. For a scalar wavelet, the number of vanishing moments

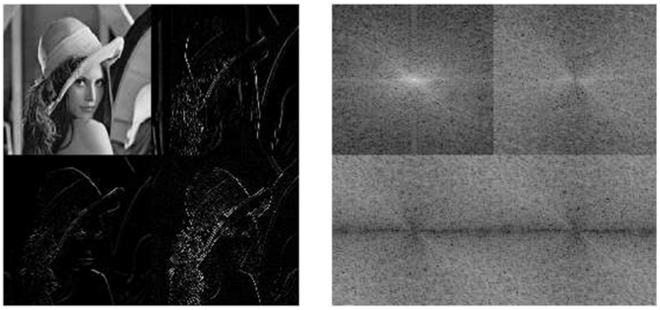

Fig. 4. Multiwavelet approximation subband of Lena image (left). Spectral densities of subband blocks L_0L_0, L_0L_1, L_1L_0 and L_1L_1 (right).

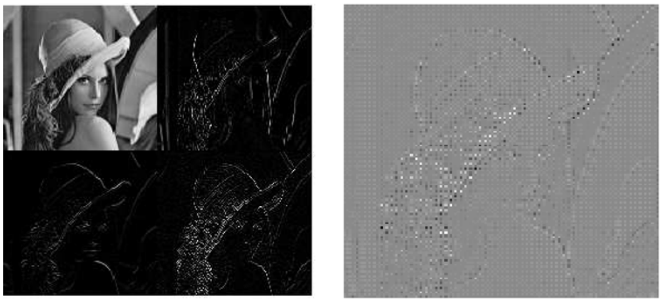
(a) (b)

Fig. 5. (a) Four sub-blocks of multiwavelet approximation subband of Lena image. (b) Shuffling effect on approximation subband.

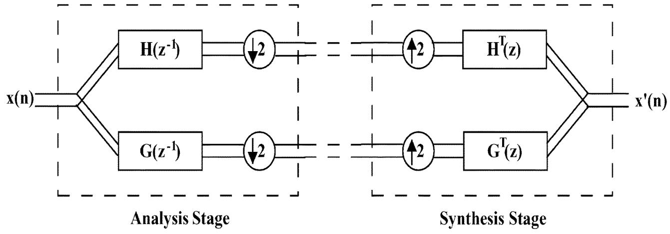

Fig. 6. Perfect reconstruction multiwavelet filter bank.

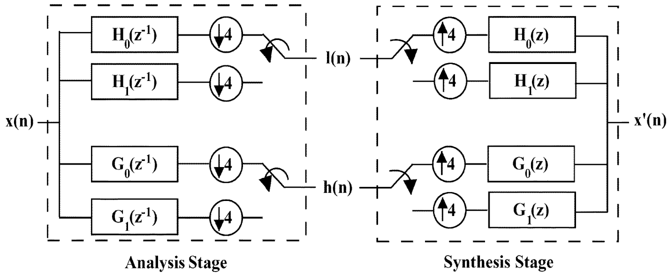

Fig. 7. Time-varying multiwavelet filter bank.

of its wavelet function $\int t^m \psi(t)dt = 0$ determines its vanishing order. For a scalar wavelet with vanishing order K, the high-pass branch cancels a monomial of order less than K and the low-pass branch preserves it. For a multiwavelet transform, we have a similar notion of approximation order; a multiwavelet is said to have an approximation order of K if the vanishing moments of its wavelets, $\int t^m \psi_i(t)dt = 0$ for $0 \leq i \leq r-1$ and $0 \leq m \leq K-1$. An approximation order of K implies that the high-pass branch cancels monomials of order less than K. However, in general, for multiwavelets, the preservation property does not automatically follow from the vanishing moments property. If the multifilter bank preserves the monomials at the low-pass branch output, the multiwavelet is said to be *balanced* [10]. The *balancing* order is p if the low-pass and high-pass branches in the filter bank preserve and cancel, respectively, all monomials of order less than p $(p \leq K)$. Multiwavelets that do not satisfy the preservation/cancellation property are said to be *unbalanced*. For unbalanced multiwavelets, the input needs suitable *prefiltering* to compensate for the absence of the preservation/cancellation property, balancing obviates the need for input prefiltering; thus, they are computationally more efficient than the unbalanced multiwavelets. In [10], the multiwavelet filter bank, shown in Fig. 6, is viewed as a time-varying filter bank.

To keep the transform nonexpansive, a polyphase vectorization is performed on the input image [10]. Therefore, the matrix filter bank, given by (4) and (5), is transformed into a simple time-varying multichannel filter bank as shown in Fig. 7. The time-varying filter bank, shown in Fig. 7, is described by (6) and (7).

$$\begin{bmatrix} H_0(z) \\ H_1(z) \end{bmatrix} = H(z^2) \begin{bmatrix} 1 \\ z^{-1} \end{bmatrix} \tag{6}$$

$$\begin{bmatrix} G_0(z) \\ G_1(z) \end{bmatrix} = G(z^2) \begin{bmatrix} 1 \\ z^{-1} \end{bmatrix} \tag{7}$$

where $H_0(z)$ and $H_1(z)$ are the z transforms of the two low-pass branch filters h_0 and h_1. Similarly, $G_0(z)$ and $G_1(z)$ are the z transforms of the two high-pass branch filters g_0 and g_1. In the time-varying filter bank implementation, the coefficients of the two low-pass (high-pass) filters are simply interleaved at the output (see Fig. 7). Therefore, a separable 2-D transform can now be defined in the usual way as the tensor product of two 1-D transforms [10]. However, in the 2-D transform case, 16 subbands are obtained instead of the usual 4 subbands with scalar wavelet transforms. For instance, for a single-level balanced multiwavelet, the four sub-blocks of the approximation subband can be combined using the shuffling method described previously. Unlike the unbalanced case (see Fig. 5), the resulting approximation subband is a "*real* " low-pass representation of the image. Fig. 8 shows the four sub-blocks of the low-pass subband of the balanced multiwavelet transform of Lena image. Unlike unbalanced multiwavelets, these sub-blocks have similar spectral characteristics as shown on the left side of Fig. 8. Furthermore, shuffling of these four sub-blocks yields a "*real*" low-pass subband, as illustrated in Fig. 9 for the case of Lena image.

2) Perceptual Model for Balanced Multiwavelet Transforms: We will give a brief overview of Chou's model and show its relevance to the balanced multiwavelet transforms[4]

---

[4] One of the major merits of this model is its independence of the wavelet kernels unlike the model proposed in [13]. Therefore, the proposed watermarking system will be valid for any kind of transform kernels.

Fig. 8. Balanced multiwavelet approximation subband of Lena image (left). Spectral densities of subband blocks L_0L_0, L_0L_1, L_1L_0, and L_1L_1 (right).

through the use of subbands' modeling. Chou and Li [9] propose a JND or minimally noticeable distortion (MND) profile to quantify the "*perceptual redundancy*." The JND profile provides a visibility threshold of distortion for each image being analyzed. The latter indicates the level below which distortions due to watermark embedding are rendered imperceptible. The JND profile incorporates two major factors, known to be influential in the human visual perception; namely the "*background luminance*" and "*texture masking effect*." The purpose of the JND profile is to guide the watermark embedding in the BMW domain. Therefore, this profile must be decomposed into component JND/MND profiles of different frequency/orientation subbands. With the decomposed profile, watermark data will be adaptively embedded into subband coefficients according to their "*perceptual significance*."

a) Perceptual redundancies: The imperfections and the inconsistency in sensitivity inherent to the human visual system (HVS) allow for "*perceptual redundancies*." Psychovision studies [14] indicate that the visibility threshold of a particular stimulus depends on many factors. There are primarily two major factors that affect the error visibility threshold of each pixel.[5]

- *Luminance contrast:* Human visual perception is sensitive to luminance contrast rather than absolute luminance value. As indicated by Weber's law, if the luminance of a test stimulus is just noticeable from the surrounding luminance, then the ratio of just noticeable luminance difference to stimulus difference, known as *Weber fraction*, is constant.
- *Spatial masking:* The second factor reflects the fact that the reduction in the visibility of the stimuli is caused by the increase in the spatial nonuniformity of the background luminance. This fact is known as *spatial masking*.

Chou's perceptual model estimates, from pixels in the spatial domain, the JND value associated with each pixel in the image. Strictly speaking, the visibility threshold of JND is a very complex process and depends of the aforementioned factors. However, in [9], the interrelevance of the two factors is simplified and the JND value is defined as the dominant effect of the two factors. The perceptual model for estimating the "*full-band JND*" profile is described by the following expressions [9]:

$$\begin{aligned}&\mathrm{JND}_{\mathrm{fb}}(x,y)\\&\quad=\max\{f_1(b_g(x,y),m_g(x,y)),f_2(b_g(x,y))\}\end{aligned}\tag{8}$$

$$\begin{aligned}&f_1(b_g(x,y),m_g(x,y))\\&\quad=m_g(x,y)\alpha(b_g(x,y))+\beta(b_g(x,y))\end{aligned}\tag{9}$$

$$\begin{aligned}&f_2(b_g(x,y))\\&\quad=\begin{cases}T_0\cdot\left(1-\left(\frac{b_g(x,y)}{127}\right)^{1/2}\right)+3 & \text{for } b_g(x,y)\le 127\\ \gamma\cdot(b_g(x,y)-127)+3 & \text{for } b_g(x,y)>127\end{cases}\end{aligned}\tag{10}$$

$$\begin{aligned}&\alpha(b_g(x,y))\\&\quad=b_g(x,y)\cdot 0.0001+0.115\end{aligned}\tag{11}$$

$$\begin{aligned}&\beta(b_g(x,y))\\&\quad=\lambda-b_g(x,y)\cdot 0.001\end{aligned}\tag{12}$$

where $b_g(x,y)$ and $m_g(x,y)$ are the average background luminance and the maximum weighted average luminance differences around the pixel at (x,y), respectively. The spatial masking effect is taken into account by the function $f_1(x,y)$, the linear behavior of which is obtained from psychovisual tests [9]. The visibility threshold due to background luminance is given by the function $f_2(x,y)$ in which the relationship between noise sensitivity and the background luminance is

---

[5] Only achromatic images in the spatial domain are considered. Hence, the JND/MND profile must be decomposed to fit a subband decomposition structure.

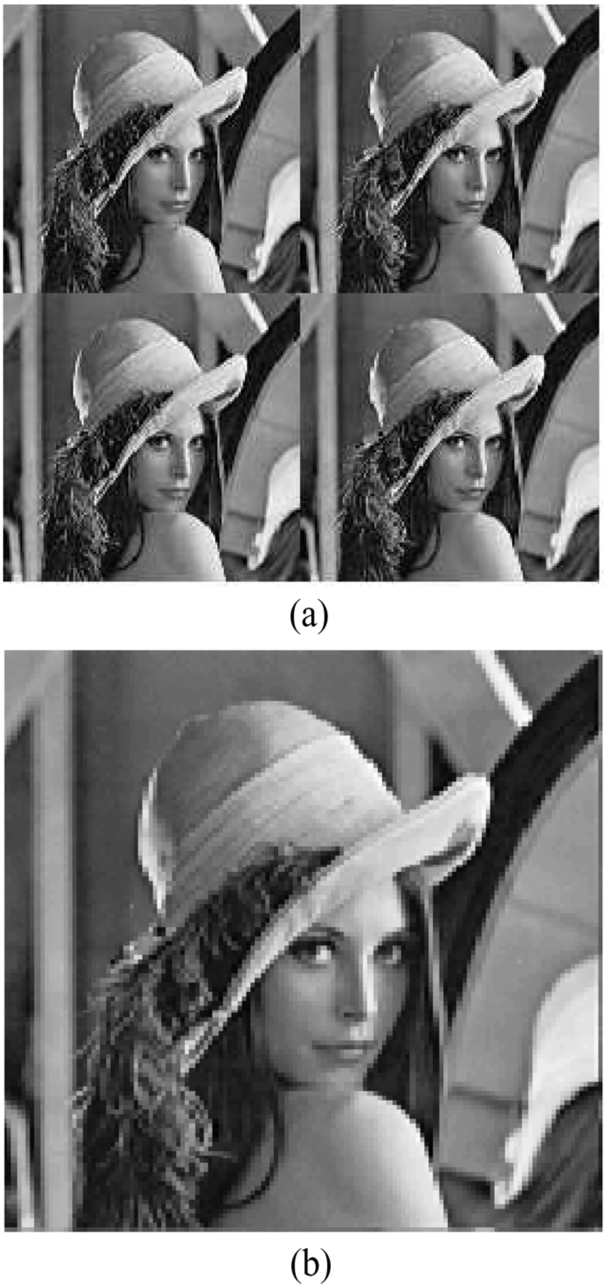

Fig. 9. (a) Four sub-blocks of balanced multiwavelet approximation subband of Lena image. (b) Shuffling effect on approximation subband.

verified by a subjective test [9]. The parameters $\alpha(x,y)$ and $\beta(x,y)$ are background-dependent functions derived through psychovisual experiments. T_0 and γ denote, respectively, the visibility threshold when the background grey level is 0, and the slope of the linear function relating the background luminance to visibility threshold at higher background luminance (level higher than 127). Parameter λ affects the average amplitude of visibility threshold due to spatial masking effect. During the conducted experiments in [9], T_0, γ, and λ are found to be 17, $(3/128)$, and $(1/2)$, respectively.

b) Deriving MND profile: To accommodate different embedding strengths, the MND profile of different distortion levels are required. In this case, the MND profile is obtained by simply multiplying every element of the JND profile, defined in (8), by a constant scale factor d as a distortion index. Thus, the MND profile with a distortion index d can be expressed as [9]

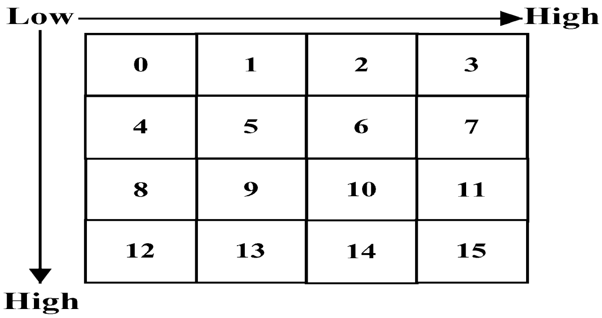

Fig. 10. Subband decomposition structure.

$$\mathrm{MND}_{d,\mathrm{fb}}(x,y) = \mathrm{JND}_{\mathrm{fb}}(x,y) \cdot d \tag{13}$$

where the value of d ranges from 1.0 to 4.0. The $m_g(x,y)$ across the pixel at (x,y) is determined by calculating the weight average of luminance changes around the pixel in four directions. Four operators $\mathbf{G_k}(i,j)$ for $i,j = 1,2,\ldots,5$, are employed to perform the calculations, where the weighting coefficient decreases as the distance away from the central pixel increases. The weight operators $\mathbf{G_k}$ are given by [9]

$$\mathbf{G_1} = \begin{bmatrix} 0 & 0 & 0 & 0 & 0 \\ 1 & 3 & 8 & 3 & 1 \\ 0 & 0 & 0 & 0 & 0 \\ -1 & -3 & -8 & -3 & -1 \\ 0 & 0 & 0 & 0 & 0 \end{bmatrix}$$
$$\mathbf{G_2} = \begin{bmatrix} 0 & 0 & 1 & 0 & 0 \\ 0 & 8 & 3 & 0 & 0 \\ 1 & 3 & 8 & -3 & -1 \\ 0 & 0 & -3 & -8 & 0 \\ 0 & 0 & -1 & 0 & 0 \end{bmatrix}$$
$$\mathbf{G_3} = \begin{bmatrix} 0 & 0 & 1 & 0 & 0 \\ 0 & 0 & 3 & 8 & 0 \\ -1 & -3 & 0 & 3 & 1 \\ 0 & -8 & -3 & 0 & 0 \\ 0 & 0 & -1 & 0 & 0 \end{bmatrix}$$
$$\mathbf{G_4} = \begin{bmatrix} 0 & 1 & 0 & -1 & 0 \\ 0 & 3 & 0 & -3 & 0 \\ 0 & 8 & 0 & -8 & 0 \\ 0 & 3 & 0 & -3 & 0 \\ 0 & 1 & 0 & -1 & 0 \end{bmatrix}. \tag{14}$$

Using the weights defined in (14), the maximum weighted average of luminance differences $m_g(x,y)$ is given by the following expression:

$$m_g(x,y) = \max_{k=1,2,3,4} \{|\mathrm{grad}_k(x,y)|\} \tag{15}$$

where

$$|\mathrm{grad}_k(x,y)| = \frac{1}{16} \sum_{i=1}^{5} \sum_{j=1}^{5} p(x-3+i, y-3+j) \cdot \mathbf{G_k}(i,j) \tag{16}$$

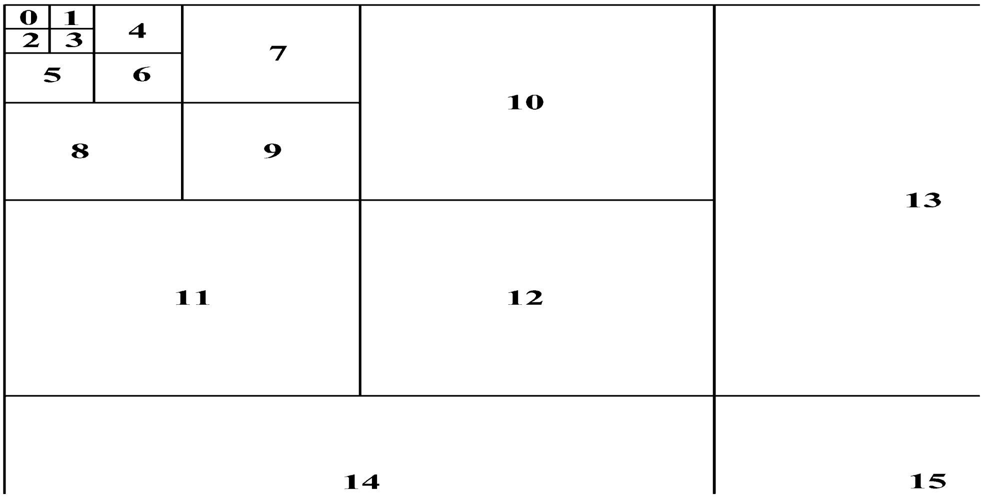

Fig. 11. JND profile structure for BMW subbands using five decomposition levels.

where $p(x,y)$ denotes the pixel at position (x,y). The average background luminance, $b_g(x,y)$, is calculated by a weighted operator $\mathbf{B}(i,j), i,j=1,2,\ldots,5$.

$$b_g(x,y)=\frac{1}{32}\sum_{i=1}^{5}\sum_{j=1}^{5}p(x-3+i,y-3+j)\cdot\mathbf{B}(i,j) \quad (17)$$

where the weight factor $\mathbf{B}(i,j)$ is given by

$$\mathbf{B}(i,j)=\begin{bmatrix}1&1&1&1&1\\1&2&2&2&1\\1&2&0&2&1\\1&2&2&2&1\\1&1&1&1&1\end{bmatrix}. \quad (18)$$

c) Decomposition of the JND/MND Profile: Since Chou's perceptual model is not aimed at watermark embedding, the JND/MND profile must be modified to accommodate the decomposition structure obtained using balanced multiwavelet transforms. For an $N \times N$ image, the JND/MND profile, as originally proposed by [9], has the linear subband structure shown in Fig. 10.

As suggested by the HVS models and human perception sensitivity, the high frequency subbands have higher weights. However, the linear decomposition structure, shown in Fig. 10, does not lend itself to such a property. Therefore, we need to find a suitable decomposition according to the frequency content of the BMW subbands. Such a solution is presented in Fig. 11. Using the BMW decomposition and the modified JND profile, Figs. 12 and 13 show the resulting JND/MND profiles of Lena and Barbara images, respectively. These figures clearly show the ability of the proposed JND/MND profile to adaptively adjust itself to the image activity. Therefore, edges and salient features are efficiently discriminated as highlighted. This property is a key factor to satisfy the imperceptibility requirement often encountered in watermarking applications [15].

Finally, the JND/MND profile should be decomposed to fit the subband structure shown in Fig. 11. The subband profile is given by

$$\mathrm{JND}_q^2(x,y)=\left[\sum_{i=0}^{3}\sum_{j=0}^{3}\mathrm{JND}_{\mathrm{fb}}^2(i+x\cdot 4,j+y\cdot 4)\right]\cdot\omega_q$$
$$\text{for } q=0,1,\ldots,15, \quad \text{and} \quad 0\le x\le \tfrac{N}{4}, \quad 0\le y\le \tfrac{N}{4} \quad (19)$$

where $\mathrm{JND}_q(x,y)$ denotes the magnitude of the JND at position (x,y) of the qth subband (see Fig. 11). The factor ω_q, representing the qth subband weight, is defined by the following expression:

$$\omega_q=\left(S_q\cdot\sum_{k=0}^{15}S_k^{-1}\right)^{-1}, \quad \text{for } q=0,1,\ldots,15 \quad (20)$$

where S_k denotes the average sensitivity of the HVS to spatial frequencies in the kth subband. The average sensitivity S_k is given by [9]

$$S_k=\frac{16}{N\cdot N}\sum_{u=\epsilon_k\cdot h}^{(\epsilon_k+1)h-1}\;\sum_{v=\rho_k\cdot w}^{(\rho_k+1)w-1}\xi(u,v)$$
$$\text{for } k=0,1,\ldots,15 \quad (21)$$

where

$$h=\frac{N}{4}, \quad w=\frac{N}{4}, \quad \epsilon_k=\left\lfloor\frac{k}{4}\right\rfloor, \quad \rho_k=k-\epsilon_k\cdot 4$$

and $\xi(u,v)$ denotes the response curve of the modulation transfer function (MTF) for $0\le u\le N, 0\le v\le N$. Chou and

Fig. 12. Lena image (left) and its resulting JND/MND profile (right).

Fig. 13. Barbara image (left) and its resulting JND/MND profile (right).

Li [9] propose the following generalized formula for fitting the response curve of the MTF:

$$\xi(u,v) = a \cdot \left[b + \left(\frac{\Omega(u,v)}{\Omega_0}\right)\right] \cdot \exp\left[-\left(\frac{\Omega(u,v)}{\Omega_0}\right)^{c}\right] \quad (22)$$

where

$$\Omega(u,v) = \left[\left(\frac{32v}{N}\right)^2 + \left(\frac{24u}{N}\right)^2\right]^{\frac{1}{2}}$$
$$\text{for } 0 \le u \le N-1, \quad 0 \le v \le N-1 \quad (23)$$

is the spatial frequency in cycles per degree (cpd) and Ω_0 is a shaping parameter for the MTF curve [9]. It should be noted that the JND profiles shown in Figs. 12 and 13 are derived for the MTF curve modeled by $a = 2.6, b = 0.0192, c = 1.1, \Omega_0 = 8.772$, $T_0 = 17$, $\gamma = (3)/(128)$, and $\lambda = (1/2)$, respectively. The distortion index d is fixed to 3.0. The BMW JND profile subbands, given by (19), are inverse-transformed to obtain the spatial JND profiles shown in Figs. 12 and 13.

C. Watermark Decoding

The problem of watermark decoding is reminiscent of the classical problem of detecting a known signal in background noise. Maximum-likelihood (ML) detection is used to extract each embedded bit from the watermarked signal coefficients. In this paper, we model the subband coefficients of the host signal using a statistical model proposed in [16] where the assumed model is a generalized-Gaussian distribution (GGD). However, the watermark detector operates in a blind fashion where the original host is not available. Therefore, the watermarked subband coefficients, themselves, are used for estimating the model parameters under the assumption that the distortion due to watermark embedding is relatively small (see assumptions about distortion D_1 in Section III). The BMW subband coefficients are modeled according to a GGD model where $f_y(y) = A\exp(-|\alpha y|^{\beta})$, where A and α depend on β and the standard deviation σ_y of the subband coefficients. The parameters A and α are defined as follows:

$$A = \frac{1}{\sigma_y}\left(\frac{\Gamma(3/\beta)}{\Gamma(1/\beta)}\right)^{1/2} \quad (24)$$

and

$$\alpha = \frac{\alpha\beta/2}{\Gamma(1/\beta)}. \quad (25)$$

At the decoder stage, we have the following hypothesis test:

$$\begin{aligned}&\text{hypothesis } H_0: && \text{a bit 0 is embedded } (m=-1)\\ &\text{hypothesis } H_1: && \text{a bit 1 is embedded } (m=1).\end{aligned}$$

The corresponding maximum log-likelihood decision rule decides for the bit to be a 1 if

$$\begin{aligned}\Delta_{\mathrm{BMW}} = &\sum_{j=1}^{\chi}\log(1-\alpha m_j)+\sum_{j=1}^{\chi}\log\left|\frac{\alpha_j y_j}{1-\alpha m_j}\right|^{\beta_j}\\ &-\sum_{j=1}^{\chi}\log(1+\alpha m_j)-\sum_{j=1}^{\chi}\log\left|\frac{\alpha_j y_j}{1+\alpha m_j}\right|^{\beta_j}\\ &\geq 0. \end{aligned} \tag{26}$$

Estimation of β and σ_y parameters is carried out independently for each embedded watermark $m_k, 1 \leq k \leq M$. It should be noted that each watermark bit is embedded into χ different host coefficients. Therefore, the decoder complexity depends mainly on the number of watermark bits being embedded. The parameters α and A can be estimated using the pair (β, σ_y). It should be noted that the ML rule, given by (26), does not require the knowledge of the parameter A. Furthermore, for a robust estimation of the parameters (β, σ_y), the number of the subband coefficients should not be less than 256 as indicated in [17]. In the proposed system, the detection is based on a correlation detector. Using the embedding formula given by (1), the corresponding correlation detector has the following form:

$$m_i = \begin{cases} -1, & \text{if } \langle x_i \cdot pni\rangle < 0\\ +1, & \text{if } \langle x_i \cdot pni\rangle \geq 0\end{cases} \tag{27}$$

where $\langle\cdot\rangle$ is the scalar product operator.

III. INFORMATION-THEORETIC DATA-HIDING ANALYSIS

To derive the fundamental limits of watermarking and data hiding systems, we will follow the framework used in [1]–[4] where no *a priori* assumptions are made about the embedding and decoding functions. The recent theory developed in [2] and [4] establishes the fundamental limits of the watermarking (and data hiding) problem. A communication-like representation of the watermarking problem is shown in Fig. 1.

A. Communications Model for Watermarking

In Moulin–Mihçak's framework [2], [4], the watermarking system embeds or hides a watermark payload message M in a length-N host data sequence $S^N = (S_1, \ldots, S_N)$. Side-information $K^N = (K_1, \ldots, K_N)$, such as cryptographic key or host signal-dependant data, may be used by the watermark embedding stage. The watermarked data is denoted by $X^N = (X_1, \ldots, X_N) = f_N(S^N, M, K^N)$. Watermark attackers, modeled by attack channels, intend to remove or at least make useless the embedded message M. The sequence $Y^N = (Y_1, \ldots, Y_N)$ represents the attacked watermarked sequence. To derive the data-hiding capacity, we assume that the host images can be "*correctly*" modeled as sequences of independent and identically distributed (i.i.d.) K-dimensional Gaussian random vectors $S \sim \mathcal{N}(0, R)$, where R is a $K \times K$ correlation matrix. In this paper, the squared Euclidean distance, $d(x, y) = \|x-y\|^2$, for $x, y \in \Re^K$ is used as the main distortion metric. Data-hiding capacity estimates for the scalar case, where $K = 1$ and $S \sim \mathcal{N}(0, \sigma^2)$, are presented in [2]. While detailed results specific to the vector case may be found in [4], a summary of these results is outlined in [2]. In this paper, we are mainly interested in the parallel representation of the outlined problem. Thus, the host data S is represented by means of K parallel Gaussian channels. In the latter case, the channel inputs are K independent sources $S_k, 1 \leq k \leq K$. Each channel S_k is modeled as a sequence of i.i.d. Gaussian random variables $\mathcal{N}(0, \sigma_k^2)$. The watermark payload message M is uniformly distributed over the message set $\mathcal{M}$ and is independent of the host signal S. Because the watermarking problem can be viewed as a game-theoretic problem between the data embedder and the attacker who is an intelligent opponent, game-theoretic analysis of the watermarking problem has been successfully formulated for both the scalar and vector cases [3], [4]. In this game-theoretic framework [4], maximum distortion levels are specified for both the watermark embedder (D_1) and attacker (D_2). The maximum expected-distortion imposed on the watermark embedder is given by [4]

$$Ed^N(S^N, X^N) \leq D_1. \tag{28}$$

Attacks on embedded watermarks, modeled by specific channel models, are subject to distortion D_2 [4]

$$Ed^N(S^N, Y^N) \leq D_2, \quad N \geq 1. \tag{29}$$

Equation (29) represents a constraint on the expected distortion with respect to the host signal S^N that the watermark attacker is willing to introduce [4]. For a specific length-N data-hiding code, the data-hiding capacity $C(D_1, D_2)$ is defined as the supremum of all achievable rates R for distortions (D_1, D_2) [4].[6]

1) Scalar Gaussian Channels: Under the distortion constraints (28) and (29), the data-hiding capacity for scalar Gaussian channels is given by [4]

$$C = \Gamma(\sigma^2, D_1, D_2) \triangleq \begin{cases} \frac{1}{2}\log\left(1+\frac{D_1}{D}\right), & \text{if } D_1 < D_2 < \sigma^2\\ 0, & \text{if } D_2 \geq \sigma^2\end{cases} \tag{30}$$

where $D \triangleq \sigma^2(D_2 - D_1/\sigma^2 - D_2)$. In practical watermarking applications where $\sigma^2 \gg D_1, D_2$, we have $D \sim D_2 - D_1$ and therefore

$$C \sim \frac{1}{2}\log\left(1+\frac{D_1}{D_2 - D_1}\right). \tag{31}$$

Equation (31) clearly indicates that the capacity is independent of the host signal variance σ^2. In addition, it is quite interesting to note that regardless of the availability of the host signal at the decoder, the same value of capacity is obtained.

---

[6] It should be noted that a rate R is achievable for distortions (D_1, D_2) if there exists a sequence of codes, subject to distortion D_1, with respective rates $R_N > R$, such that the probability of error P_e tends to zero as $N \to \infty$ [4].

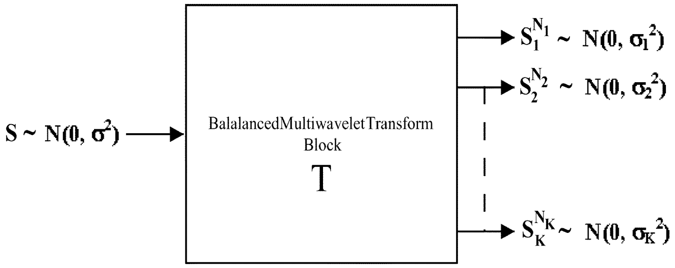

Fig. 14. Host signal representation using parallel Gaussian channels.

2) Parallel Gaussian Channels: In this paper, the parallel Gaussian case is of interest to us. Fig. 14 illustrates the concept of the problem representation using parallel Gaussian channels. The host signal S^N is decomposed into K channels using the balanced multiwavelet transform. Each host subsignal $S_k^{N_k}$, $1 \leq k \leq L$ consists of N_k samples. According to the model assumptions presented earlier, the subsignals $S_k^{N_k}$ are independent and are assumed to be Gaussian-distributed such as $\mathcal{N}(0, \sigma_k^2)$.

Let d_{1k} and d_{2k} be the distortions introduced in channel k by the watermark embedder and attacker, respectively. Moulin and Mihçak [4] show that the allocation of powers $d_1 = \{d_{1k}\}$ and $d_2 = \{d_{2k}\}$ between channels, satisfies the overall distortion constraints

$$\sum_{k=1}^{K} r_k d_{1k} \leq D_1 \tag{32}$$

$$\sum_{k=1}^{K} r_k d_{2k} \leq D_2 \tag{33}$$

where r_k is the inverse subsampling factor in channel k given by: $r_k = (N_k)/(N)$. It is assumed that $\sum_{k=1}^{K} r_k = 1$. (32) and (33) are subject to the following $3K$ constraints:

$$0 \leq d_{1k} \tag{34}$$

$$d_{1k} \leq d_{2k} \tag{35}$$

$$d_{2k} \leq \sigma_k^2 \tag{36}$$

for $1 \leq k \leq K$. The data-hiding capacity of parallel Gaussian channels is defined by the maximization–minimization relation, given by (37), subject to the $3K + 2$ constraints shown above [4], as follows:

$$C = \max_{d_1} \min_{d_2} \sum_{k=1}^{K} r_k \Gamma\left(\sigma_k^2, d_{1k}, d_{2k}\right) \tag{37}$$

Moulin and Mihçak [4] provide a numerical optimization algorithm to compute the capacity in (37).

B. Models of Typical Images

Unlike in the case of unbalanced multiwavelets, the structure of the subbands emanating from balanced multiwavelet decomposition have similar structure to that obtained using scalar wavelet decomposition (refer to Section II-B-1) for details). This similarity in subband structure motivates us to investigate the suitability of well-established statistical models that were initially designed for scalar wavelets. In these models [18] and [16], subbands' coefficients are modeled as Gaussian and generalized-Gaussian processes, respectively, with zero means and variances that depend on the coefficient location within each decomposition subband. In [18], it is assumed that the coefficients' variances belong to a finite set of values $\sigma_k^2, 1 \leq k \leq K$. Joshi *et al.* [18] recommend a typical value of K equal to eight times the number of decomposition subbands. The estimation-quantization (EQ) model, proposed by Lopresto *et al.* [16], assumes that the coefficients' variances are random and slowly varying such that the decoder can reliably estimate their values. In this paper, we will use the technique proposed in [4] to estimate representative values of $\sigma_k^2, 1 \leq k \leq K$. The technique is described below for convenience.

1) Apply balanced multiwavelet transform to a representative image of a typical class using five decomposition levels.
2) Estimate the local variance in a 5 × 5 window centered at each wavelet coefficient.
3) Quantize the natural logarithm of each of these variance estimates using a uniform quantizer with K levels and quantizer step size Δ. Then, a watermarking Gaussian channel consists of all coefficients having the same quantized variance within each subband.

In this paper, we present simulation results and capacity estimates for watermark embedding using $K = 256$ channels. Also, we investigate the case of $K = 64$ to provide an equal-foot and fair comparison with the block-based DCT watermarking paradigm.[7] Figs. 15 and 16 show the resulting 256 parallel channels to accommodate watermark embedding in Lena and Baboon images, respectively. Dark regions (approximation and detail subbands at level 5) represent perceptually important image regions. In these figures, the estimated variances, and therefore channels, are consistent with the notion, originally formulated by Cox *et al.* [19], that "*watermarks should be embedded in perceptually and significant signal components*." On the other hand, we note that coefficients of the low-pass subband, correctly classified as high variance channels, are characterized with higher embedding capacities. Based on this, it is clear that skipping the most perceptually dominant signal components, as recommended in [19], results in a drastic decrease in data-hiding capacity. It should be noted that under mild attacks, some of the perceptually less important channels (see Figs. 15 and 16) will move away from their original positions. However, due to repetition-encoding of the watermark payload, most of the affected channels can be safely recovered. Fig. 17 illustrates the solution of (37) to derive the capacity per sample in each of the 256 channels for Lena image assuming an attacker distortion fixed at $D_2 = 2D_1$. The capacity estimates are related to the embedding channels shown in Fig. 15. For comparison purposes, capacity estimates yielded by scalar Daubechies-8 (Daub8) wavelet transform [4] are also provided. It is clear that BMW transform is characterized by higher data-hiding capacity. The increase in the embedding rate could be efficiently used to inject synchronization data in the host medium to combat desynchronization attacks.

---

[7] In block-based DCT watermarking systems, an 8 × 8 block DCT yields 64 parallel channels.

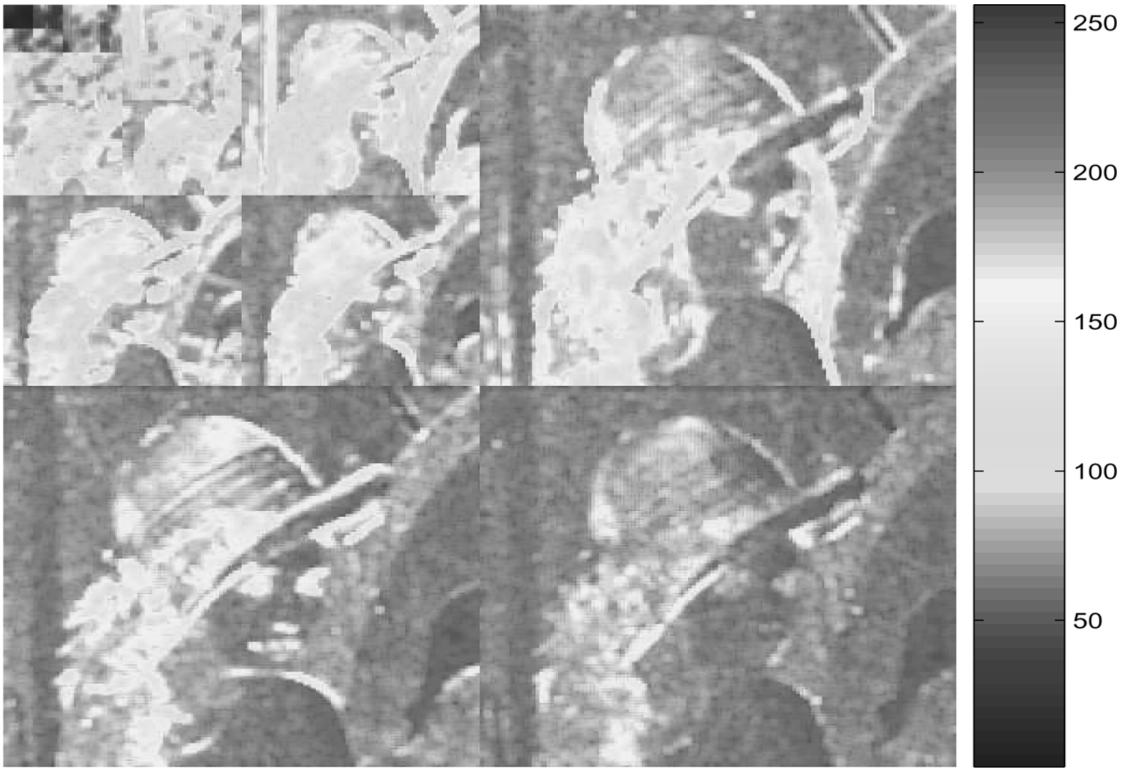

Fig. 15. EQ-estimated 256 parallel Gaussian channels in Lena image.

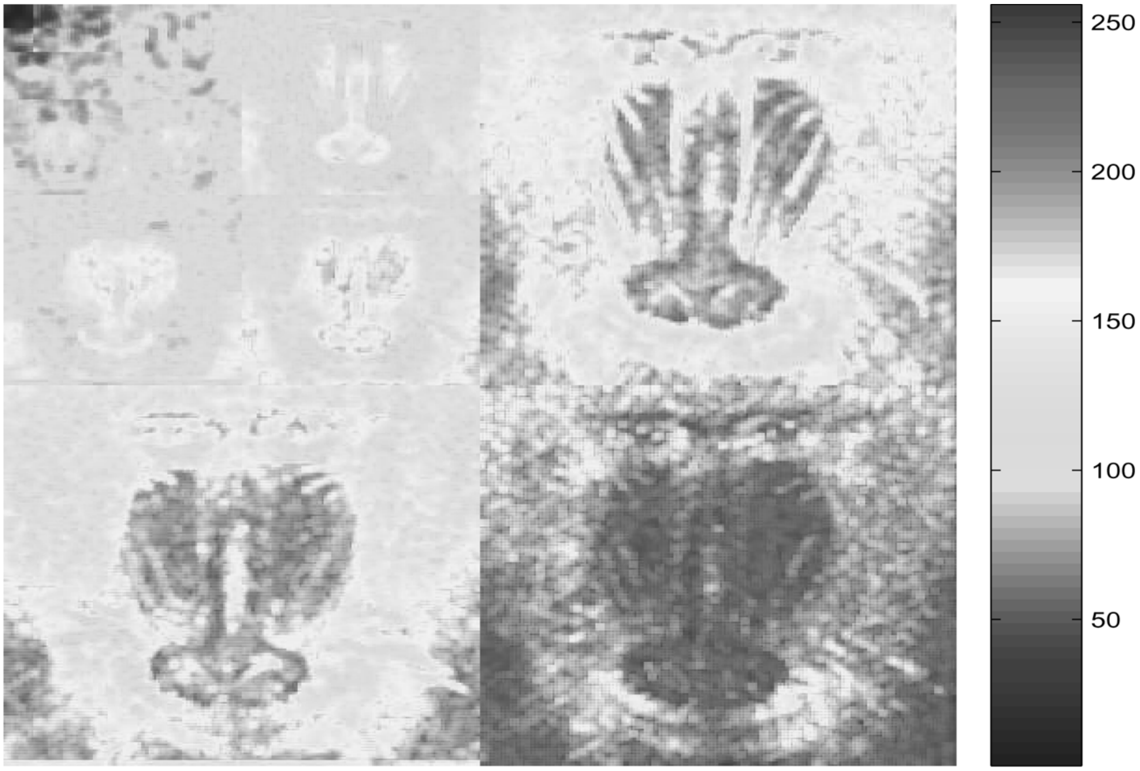

Fig. 16. EQ-estimated 256 parallel Gaussian channels in Baboon image.

C. *Estimates of Data-Hiding Capacities*

In this section, we investigate the data-hiding capacity of typical natural test images. Analysis results are presented for four test images, Lena, Barbara, Baboon, and Peppers. The original test images are shown in Fig. 18.

We perform a simple subjective evaluation to estimate the value for D_1 for the test images such that distortion due to data embedding is just noticeable. The experiment consists of incrementally adding white noise to a test image until it becomes noticeable. Fig. 19 shows the experimental setup. Similar to [4],

TABLE I
TOTAL DATA-HIDING CAPACITIES (IN BITS) FOR IMAGES OF SIZE $N \times N = 512 \times 512$ USING ORTHOGONAL DAUBECHIES $8, 9/7$ LINEAR-PHASE FILTERS, AND BAT-1 BALANCED MULTIFILTERS

Image	D_1	$D_2 = 2D_1$		$D_2 = 5D_1$	
		NC	NC-Spike	NC	NC-Spike
Lena (Daub-8)	10	27664	22080	3677	4818
Lena (9/7 Linear phase filters)		27233	21714	3651	4589
Lena (BMW BAT-1 multifilters)		**31786**	**25820**	**4578**	**5642**
Baboon (Daub-8)	25	26347	26148	4018	5455
Baboon (9/7 Linear phase filters)		24212	25218	3781	5842
Baboon (BMW BAT-1 multifilters)		**35041**	**33578**	**5468**	**6734**
Peppers (Daub-8)	10	19422	20708	3042	4344
Peppers (9/7 Linear phase filters)		16922	17852	2790	3962
Peppers (BMW BAT-1 multifilters)		**20030**	**19774**	**3170**	**4440**
Barbara (Daub-8)	20	22840	24495	3683	5475
Barbara (9/7 Linear phase filters)		18289	20026	2868	4531
Barbara (BMW BAT-1 multifilters)		**29910**	**31134**	**4969**	**6792**

TABLE II
COMPARISON OF TOTAL DATA-HIDING CAPACITIES (IN BITS) USING 64 CHANNELS 8×8 BLOCK DCT AND BAT-1 BALANCED MULTIFILTERS

Image	D_1	$D_2 = 2D_1$		$D_2 = 5D_1$	
		NC	NC-Spike	NC	NC-Spike
Lena (Block DCT: $K = 64$)	10	**48178**	**39747**	**7922**	**7768**
Lena (BMW BAT-1 multifilters)		31786	25820	4578	5642
Baboon (Block DCT: $K = 64$)	25	30354	28391	5829	7768
Baboon (BMW BAT-1 multifilters)		**35041**	**33578**	**5468**	**6734**
Peppers (Block DCT: $K = 64$)	10	**28071**	**20708**	**5453**	**6854**
Peppers (BMW BAT-1 multifilters)		20030	19774	3170	4440
Barbara (Block DCT: $K = 64$)	20	**34925**	**35489**	**7198**	**8682**
Barbara (BMW BAT-1 multifilters)		29910	31134	4969	6792

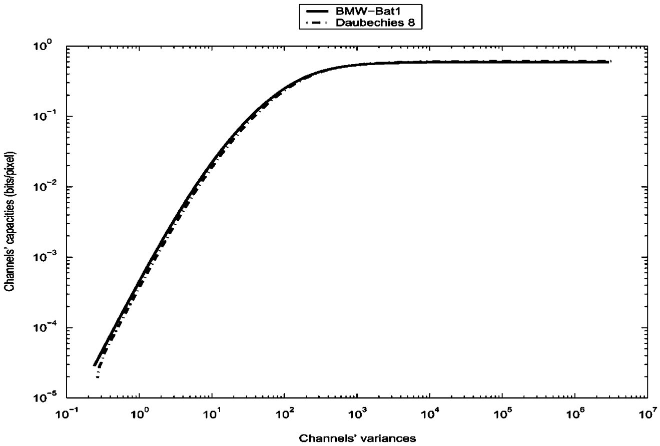

Fig. 17. Channels' contribution to capacity for Lena image ($D_1 = 10$ and $D_2 = 20$) using BMW-EQ model (solid line) and Daub8-EQ model (dashed–dotted line) [4].

Fig. 18. Original test images. Upper left: Lena. Upper right: Barbara. Lower left: Baboon. Lower right: Peppers.

the values of D_1 are 10 , 20, 25, and 10 for Lena, Barbara, Baboon, and Peppers, respectively.

To derive the fundamental limits of watermarking and data hiding systems, we will follow the methodology used in [1]–[4] where no *a priori* assumptions are made about the embedding and decoding functions. The watermarking (or data-hiding) problem, viewed as communications through noisy single or parallel Gaussian channels, has theoretical limits on the achievable capacity [2], [4]. Data-hiding capacities (NC) for the test images are shown in Table I. The displayed values represent the total data-hiding capacities (in bits) for images of size $N \times N = 512 \times 512$. In the same table, we indicate the data-hiding capacities assuming a spike model (NC-Spike) [20], where the MBW subband coefficients are classified into two different classes using a coarse quantization with threshold equal to $2D_2$.

Distortion D1 = 12.8525

Attack Variance: 12.8164

Fig. 19. Subjective estimation of D_1 levels for the test images.

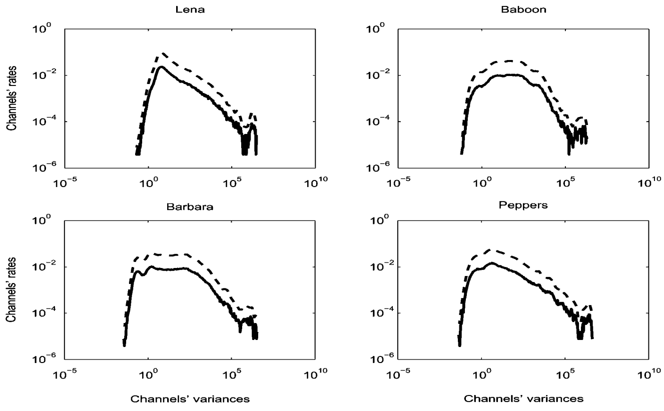

Fig. 20. Subsampling factors (on a log scale) for the test images using $K = 256$ (solid line) and $K = 64$ (dashed line) channels.

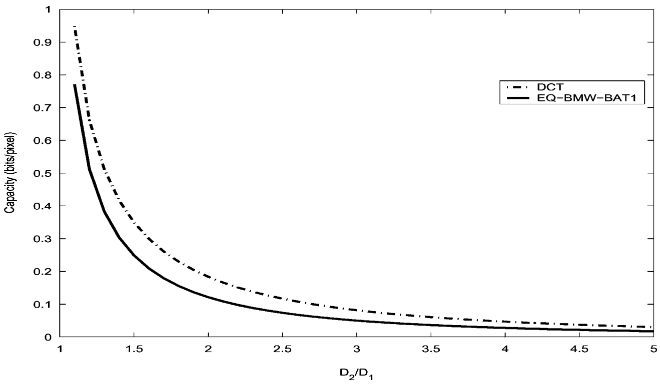

Fig. 21. Capacity in bits per pixel versus D_2/D_1 for BMW-EQ model (solid line) and block DCT model (dashed–dotted line) for Lena image.

It is clear from Table I that the proposed watermarking system yields higher data-hiding capacity due to the inherent structure of BMW transforms [21]. The ability to allow more embedding capacity is mainly due to the energy compaction property of BMW transforms. In some transforms of this class, the low-pass filters introduce a 0.5 pixel shift at each decomposition iteration, due to their structure and the signal extension scheme (symmetric border extension). Therefore, high energy coefficients at image discontinuities will be less aligned across scales. In this case, the variance estimates yield watermark channels with increased embedding capacity. The subsampling factors r_k for the cases of $K = 256$ and $K = 64$ are given in Fig. 20. In Fig. 20, each channel, characterized by a specific quantized variance, is willing to carry a specific number of bits per pixel. It is quite interesting to note that Baboon and Barbara images offer more high embedding channels due to their "*dominant*" textured nature.

Fig. 22. Additional test images used for performance evaluation.

The range of the log-variances of the subbands' coefficients controls the product $K\Delta$. The choice of $K = 256$ is motivated by the convergence of the data-hiding capacity to a limiting case [4] when Δ takes a small value ($\Delta = 0.07$ for $K = 256$).

1) Block DCT Versus BMW EQ Model: Table II gives a comparison between the capacity estimates of the proposed watermarking system and the block DCT model. It is clearly indicated that the latter yields capacity estimates higher than the former. However, in typical images, the Gaussianity assumption is quite loose, and therefore, these capacity estimates represent only upper bounds on the actual capacities [4]. Unlike all the cases shown, the BMW-based model outperforms the block DCT model for the case of Baboon image. This performance may be attributed to the ability of BMW transforms to better model textured images [22].

For a consistent comparison, we conduct an experiment to evaluate the data-hiding capacity for various levels of attacker distortion D_2. Fig. 21 shows the capacity estimates for the BMW-EQ and block DCT models for a range of attacker distortion $D_2 \in [2D_2, 5D_1]$ for the case of Lena image. Results shown are in total agreement with those summarized in Table II.

IV. SIMULATION RESULTS

We run experiments to evaluate the performance of the proposed watermarking system using the test images shown in Figs. 18 and 22.[8]

In addition, we provide comparison with another system based on block DCT model [23], [24]. Furthermore, using extensive simulation, performance evaluations are carried out to investigate the effects of the following.

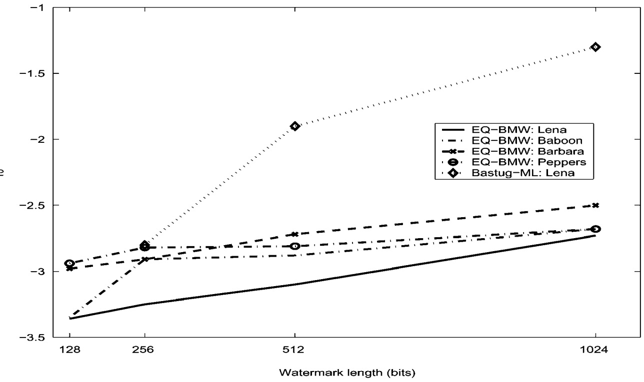

Fig. 23. Logarithmic BERs of repetition-coding using BMW method and block DCT for various watermark lengths ($M = 128$, 256, 512, and 1024).

- *Detector structure*: We present simulation results to show the improved performance of the proposed watermarking algorithm using a simple correlation detector. For comparison purposes, we provide also results obtained using an existing ML-based detector watermarking algorithm.
- *Coding strategy*: This comparison includes repetition coding versus error-correcting codes (ECCs) such as Bose–Chaudhuri–Hochquenghem (BCH) and Hamming codes.
- *Embedding domain*: Comparison of the performance of the cover media and their respective data-hiding capacity. Specifically, we investigate the robustness of the cover media provided by the BMW-EQ (see Section III) and block DCT models [23], [24]. Furthermore, we present simulation results for the proposed system robustness against typical attacks such as additive white Gaussian noise (AWGN), median filtering, Wiener filtering, and JPEG compression.

A. Performance of Uncoded Watermarks

First, we present results of the performance of the proposed system where we assume no attacks against the embedded watermarks. The embedded watermark messages consist of 128,

---

[8] To assess the performance variability with respect to content, we use ten other images obtained from the USC image database, [online] available: http://sipi.usc.edu/database/

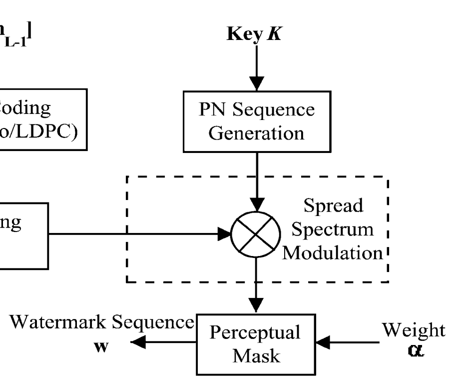

Fig. 24. ECC-encoding of the watermark information data $\mathbf{m}$.

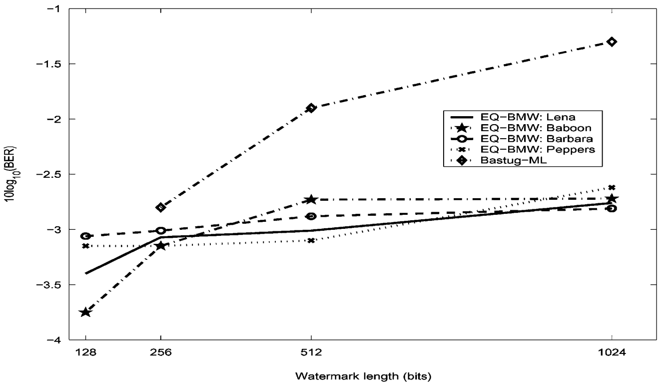

Fig. 25. Logarithmic BERs of Hamming (7, 4) code using BMW method and block DCT for various watermark lengths (M = 128, 256, 512, and 1024).

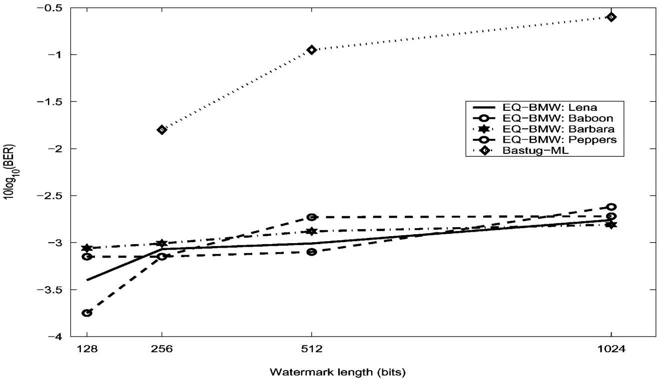

Fig. 26. Logarithmic BERs of BCH (15, 7) code using BMW method and block DCT for various watermark lengths (M = 128, 256, 512, and 1024).

256, 512, and 1024 bits, respectively. It should be noted that code repetition is employed to increase the output signal-to-noise ratio (SNR) at the decoder stage [23]. Fig. 23 shows the bit error rate (BER) of the proposed watermarking system using the EQ-BMW model. It is clear that the proposed system outperforms that based on a block DCT model [23].It is worth noting that while the block DCT model performs watermark decoding using an ML detector described by a relation similar to (26), the detector of the proposed system is based on a simple correlation measure [19]. In both cases, the embedding strategy is concerned with a scalar Gaussian channel i.e., the data-hiding capacity bound is given by (30). As expected, balanced multiwavelets provide a more robust cover medium for watermarking applications.

B. Performance of Error-Control Coded Watermarks

ECC codes are playing an important role in data-hiding and watermarking systems [24], [23]. We investigate the performance of ECC codes for watermark payload augmentation. Fig. 24 illustrates the process of ECC-encoding of the information data $\mathbf{m}$. To enhance the protection of the watermark message and improve the payload size, we will use ECC coding. However, due to the small size of the watermarking codes, we restrict ourselves to Hamming and BCH codes.[9] The performance of Hamming and BCH codes has been tested through extensive simulation using the same set of test images shown in Fig. 18.

Fig. 25 show results of the performance of the Hamming $(7, 4)$ code to protect embedded watermarks of lengths 128, 256, 512, and 1024, respectively. Also, we report results for the ML-based decoder using the block DCT model [23]. As expected, the proposed scheme is characterized by an improved decoding performance. Furthermore, the increased performance is achieved at a computational complexity similar to that of the system used in [23].

Similar to [23], we study the performance of the BCH (15, 7) code for correcting errors in the decoded watermark sequences. Fig. 26 shows the BER at the detector output. For comparison purposes, we present performance results of the ML-based detector, given in [23], for decoding watermark messages of length 256, 512, and 1024, respectively. However, it should be noted that the decoder, used in [23], is based on a BCH (63, 30) code. Again, as in the case of Hamming codes, the proposed system using the EQ-BMW model outperforms its counterpart based on the block DCT model.

C. Robustness Against Typical Attacks

Finally, we present results for the study of the robustness of the proposed watermarking system against typical attacks namely AWGN noise, median filtering, Wiener filtering, and JPEG compression. In Fig. 27, we show results for the performance of the correlation decoder in the presence of AWGN noise. We report results for the mean performance using the test images shown in Figs. 18 and 22. The watermark messages are of length 128, 256, 512, and 1024, respectively.

The results shown clearly indicate that the proposed system is able to withstand AWGN attacks. However, we notice a decrease in performance for larger watermark messages, say 1024. This decrease is mainly due to the reduction in the chirp rate χ to accommodate the upper bound of the number of embedable watermark bits [23]. It should be noted that higher values of χ yield higher SNR values at the decoder stage.

Using the same watermark lengths, results for the robustness of the proposed system against median filtering are shown in Fig. 28. The median filtering is applied locally using a window of size 3 × 3, 5 × 5, and 7 × 7, respectively.

---

[9] At small sizes, various ECC codes yield similar performance [24].

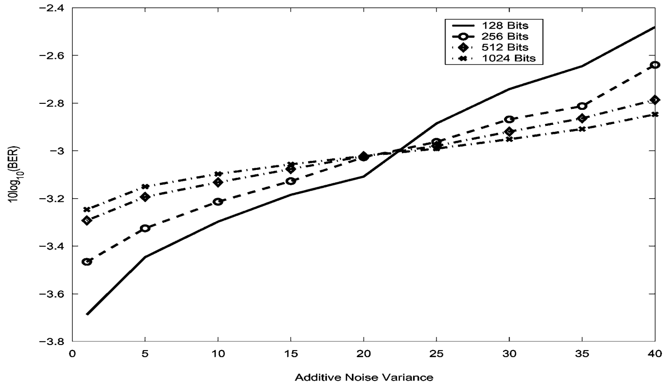

Fig. 27. Mean logarithmic BERs of BCH (15, 7) code in the presence of AWGN noise using watermark lengths of 128, 256, 512, and 1024 bits, respectively.

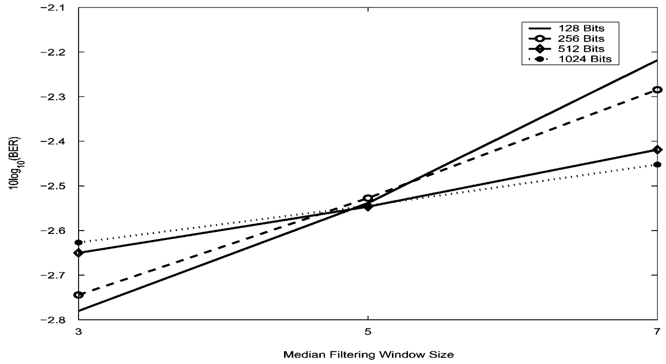

Fig. 28. Mean logarithmic BERs of BCH (15, 7) code in the presence of median filtering using watermark lengths of 128, 256, 512, and 1024 bits, respectively.

Similar to the case of AWGN noise, the system robustness against median filtering decreases for larger watermark messages. Also, for larger window sizes (5 and 7), the system performance decreases and the probability of error gets above 10^{-3} which may considered as an unacceptable performance for specific watermarking applications.

Fig. 29 illustrates results for the mean performance of the decoder in the presence of Wiener filtering.[10] Similar to the previous attacks, the watermark messages are of length 128, 256, 512, and 1024, respectively.

As expected, the Wiener filtering attack is more effective against watermarking systems. In fact, Wiener filtering may be considered as *optimal* for attacking watermark systems.

Finally, we present results for the performance of the proposed watermarking system in the presence of JPEG compression. For messages of length 128, 256, 512, and 1024, Fig. 30 shows the BERs of the watermark decoder in the presence of JPEG compression, respectively.

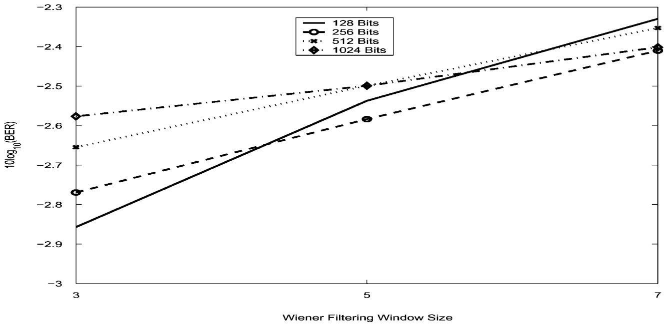

Fig. 29. Mean logarithmic BERs of BCH (15, 7) code in the presence of Wiener filtering using watermark lengths of 128, 256, 512, and 1024 bits, respectively.

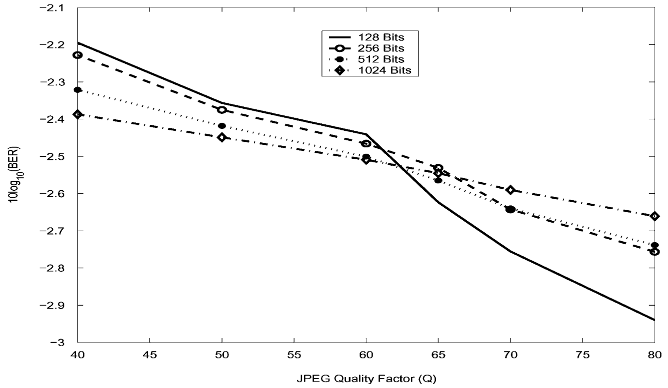

Fig. 30. Mean logarithmic BERs of BCH (15, 7) code in the presence of JPEG compression using watermark lengths of 128, 256, 512, and 1024 bits, respectively.

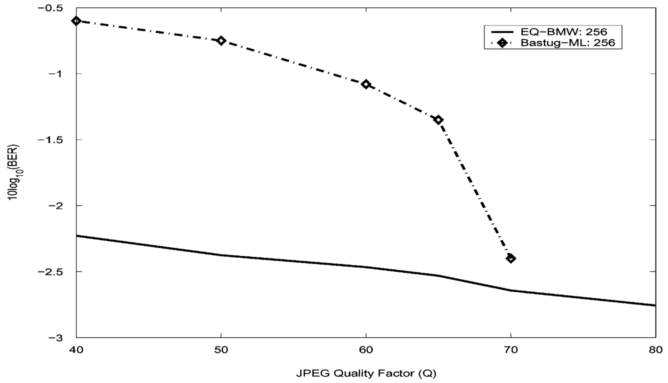

Fig. 31. Performance comparison between proposed system and the scheme of [23] for watermark message lengths of 256 bits.

The robustness of the proposed system against JPEG compression is clearly demonstrated in Fig. 30. To illustrate the high performance of the proposed system, Fig. 31 gives a comparison between the performance of the proposed system and that of the scheme used in [23]. For comparison purposes, we report results for only the case of watermark message lengths of 256 bits. Though DCT-based systems such as that in [23] offer higher embedding capacities, the proposed system exhibits higher robustness especially for low values of the JPEG quality factor Q. This improved robustness against the compression attack is mainly due to the incorporation of the perceptual model that was initially designed for image compression applications [9].

V. CONCLUSION

In this paper, we have presented a novel public image-adaptive watermarking system using the emerging BMW transform. Unlike with image coding applications, it has been demonstrated that the inherent structure of BMW decomposition

---

[10] For median and Wiener filtering, we have used Matlab built-in functions *wiener2* and *medfilt2*.

could be used constructively to achieve higher data-hiding capacities. Furthermore, we analyzed an existing subband perceptual image model and derived a convenient structure to estimate the JND profiles for BMW subbands to perceptually embed the watermark data into the host image. Unlike most of the existing perceptual models, the proposed BMW-based perceptual model is independent of the multifilter set used in the BMW transform. Also, in the course of our investigation, it was shown that that the proposed system achieves higher data-hiding capacities for the case of the parallel Gaussian watermarking channels. The gain in data-hiding capacities could be effectively used to design side channels to convey watermark synchronization signals to combat desynchronization attacks. Comparison with existing models based on scalar wavelets clearly shows the capacity gains. Finally, the performance of the novel watermarking system is presented where the robustness against typical watermark attack channels, such as AWGN noise, JPEG compression, median and Wiener filtering, is highlighted. Also, it has been demonstrated that possible improvement in watermark payload size could be achieved using error-control coding techniques such as simple repetition coding, Hamming codes, and BCH codes.

ACKNOWLEDGMENT

The authors would like to thank Dr. K. Mihçak for developing the optimization algorithm and providing valuable help during the preparation of this paper and Prof. P. Moulin for leading the research efforts of information-theoretic watermarking on which parts of this work are based. L.Ghouti acknowledges the generous support provided by KFUPM University.

REFERENCES

[1] P. Moulin and J. A. OSullivan, “Information-theoretic analysis of information hiding,” *IEEE Trans. Inf. Theory*, vol. 49, no. 3, pp. 563–593, Mar. 2003.

[2] P. Moulin and M. C. Mihçak, “A framework for evaluating the data-hiding capacity of image sources,” *IEEE Trans. Image Process.*, vol. 11, no. 9, pp. 1029–1042, Sep. 2003.

[3] A. S. Cohen and A. Lapidoth, “The Gaussian watermarking game,” *IEEE Trans. Inf. Theory*, vol. 48, no. 6, pp. 1639–1667, Jun. 2002.

[4] P. Moulin and M. C. Mihçak, “The Parallel-Gaussian watermarking game,” *IEEE Trans. Inf. Theory*, vol. 50, no. 2, pp. 272–289, Feb. 2004.

[5] I. J. Cox, M. L. Miller, and A. L. McKellips, “Watermarking as communications with side information,” *Proc. IEEE*, vol. 6, no. 7, pp. 1127–1141, Jul. 1999.

[6] S. I. Gel’fand and M. S. Pinsker, “Coding for channel with random parameters,” *Probl. Control Inf. Theory*, vol. 9, no. 1, pp. 19–31, 1980.

[7] B. Chen and G. W. Wornell, “Quantization index modulation: A class of provably good methods for digital watermarking and information embedding,” *IEEE Trans. Inf. Theory*, vol. 47, no. 5, pp. 1423–1443, May 2001.

[8] M. H. M. Costa, “Writing on dirty paper,” *IEEE Trans. Inf. Theory*, vol. 29, no. 3, pp. 438–441, May 1983.

[9] C.-H. Chou and Y.-C. Li, “A perceptually tuned subband image coder based on the measure of just-noticeable distortion profile,” *IEEE Trans. Circuits Syst. Video Technol.*, vol. 5, no. 6, pp. 467–476, Dec. 1995.

[10] J. Lebrun and M. Vetterli, “Balanced multiwavelets: Theory and design,” *IEEE Trans. Signal Process.*, vol. 46, no. 4, pp. 1119–1125, Apr. 1998.

[11] G. Strang and T. Nguyen, *Wavelets and Filter Banks*. Cambridge, U.K.: Wellesley-Cambridge, 1996.

[12] M. B. Martin and A. E. Bell, “New image compression techniques multiwavelets and multiwavelet packets,” *IEEE Trans. Image Process.*, vol. 10, no. 4, pp. 500–510, Apr. 2001.

[13] A. B. Watson, G. Yang, J. Solomon, and J. Villasenor, “Visibility of wavelet quantization noise,” *IEEE Trans. Image Process.*, vol. 6, no. 8, pp. 1164–1175, Aug. 1997.

[14] K. H. Zou, T. R. Hsing, and J. G. Dunham, “Applications of physiological human visual system model to image compression,” *Proc. SPIE*, vol. 504, pp. 419–424, 1984.

[15] I. J. Cox and M. L. Miller, “A review of watermarking and the importance of perceptual modeling,” *Proc. SPIE*, vol. 3016, pp. 92–99, 1997.

[16] S. Lopresto, K. Ramchandran, and M. T. Orchard, “Image coding based on mixture modeling of wavelet coefficients and a fast estimation-quantization framework,” in *Proc. Data Compression Conf., 97*, Snowbird, UT, 1997, pp. 221–230.

[17] M. N. Do and M. Vetterli, “Wavelet-based texture retrieval using generalized Gaussian density and Kullback–Leibler distnce,” *IEEE Trans. Image Process.*, vol. 11, no. 2, pp. 146–158, Feb. 2002.

[18] R. L. Joshi, H. Jafarkhani, J. H. Kasner, T. R. Fischer, N. Farvardin, M. W. Marcellin, and R. H. Bamberger, “Comparison of different methods of classification in subband coding of images,” *IEEE Trans. Image Process.*, vol. 6, no. 11, pp. 1473–1486, Nov. 1997.

[19] I. J. Cox, J. Kilian, F. Leighton, and T. Shamoon, “Secure spread spectrum watermarking for multimedia,” *IEEE Trans. Image Process.*, vol. 6, no. 12, pp. 1673–1687, Dec. 1997.

[20] C. Weidmann, J. Lebrun, and M. Vetterli, “Significance tree image coding using balanced multiwavelets,” in *Proc. IEEE Int. Conf. Image Processing*, vol. 2, 1998, pp. 1151–1154.

[21] C. Weidmann and M. Vetterli, “Rate-distortion analysis of spike processes,” presented at the Data Compression Conf., Snowbird, UT, Mar. 1999.

[22] L. Ghouti, A. Bouridane, and M. K. Ibrahim, “Image compression using texture modeling,” presented at the IEEE Int. Symp. Circuits Systems, Kobe, Japan, May 2005.

[23] A. Baştuğ and B. Sankur, “Improving the payload of watermarking channels via LDPC coding,” *IEEE Signal Process. Lett.*, vol. 11, no. 2, pp. 90–92, Feb. 2004.

[24] S. Baudry, J. F. Delaigle, B. Sankur, B. Macq, and H. Maitre, “Analyzes of error correction strategies for typical communication channels in watermarking,” *Signal Process.*, vol. 81, no. 6, pp. 1239–1250, Jun. 2001.

Lahouari Ghouti (S’00–M’05) was born in Oran, Algeria. He received the B.S. degree (1st Hons.) in telecommunications engineering from the Algerian Telacommunications Institute, Oran, Algeria, in 1992, the M.S. degree in electrical engineering from King Fahd University of Petroleuym and Minerals, Saudi Arabia, in 1997, and the Ph.D. degree in computer science from Queen’s University of Belfast (QUB), U.K., in 2005.

For three years, he worked as a Telecommunications Engineer at the Algerian Telecommunications Ministry. Currently, he is with the Speech and Vision Systems Group at the Institute of Electronics, Communications and Information Technology (ECIT), QUB. He has eight pending patent applications. His research interests include watermarking technologies, information hiding, content identification, multimedia security, biometrics, and signal/image processing applications for forensic and homeland security.

Dr. Ghouti is a Member of the IEEE Signal Processing Society.

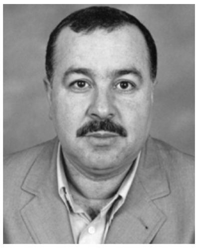

Ahmed Bouridane (M’97) received the “Ingenieur d’Etat” degree in electronics from Ecole Nationale Polytechnque of Algiers (ENPA), Algeria, in 1982, the M.Phil. degree in electrical engineering (VLSI design for signal processing) from the University of Newcastle-Upon-Tyne, U.K., in 1988, and the Ph.D. degree in electrical engineering (computer vision) from the University of Nottingham, U.K., in 1992.

From 1992 to 1996, he worked as a Research Developer in telesurveillance and access control applications. In 1994, he joined Queen’s University Belfast, Belfast, U.K., initially as Lecturer in computer archiecture and image processing. He is now a Reader in computer science, and his research interests are in high-performance image/signal processing, image/video watermarking, custom computing using field-programmable gate arrays (FPGAs), computer vision and high-performance architectures for image/signal processing. He has authored and coauthored more than 100 publications.

Dr. Bouridane is a Member of IEEE Signal Processing, Circuits and Systems, and Computer Societies.

Mohammad K. Ibrahim (S'04–M'93–SM'98) received the B.Sc. and Ph.D. degrees from the University of Newcastle-Upon-Tyne, U.K., in 1982 and 1985, respectively.

From 1982 to 1985, he was an Overseas Research Student Award holder and held a BT Short Term Fellowship during summer 1986. He held academic positions at Nottingham University, U.K., and King Fahd University of Petroleum and Minerals, Saudi Arabia, as Professor of Computer Engineering. He is currently Professor of Information and Systems Engineering, De Montfort University, Leicester, U.K. He was a visiting Professor at the Department of Computer Science, Queens University Belfast, Belfast, U.K. His research interests are in computer arithmetic, signal and image processing, cryptosystems, and application specific processors. He holds two U.S. patents and has more than 30 pending patent applications. He also has more than 110 technical publications in journals and conferences. He is the Co-Guest Editor of three special issues in the *Journal of VLSI Signal Processing Systems*.

Dr. Ibrahim is a Member of the Institution of Electrical Engineers (IEE). He is a Member of two technical committees of the IEEE Circuits and Systems Society, namely VLSI Systems and Applications and Multimedia Systems and Applications. He is also a Member of the IEEE Signal Processing Society Technical Committee on Design and Implementation of Signal Processing Systems. He currently serves on the editorial board of the IEEE TRANSACTIONS ON VLSI SYSTEMS and the *Journal of VLSI Signal Processing Systems*. He was a Member of the IEE Professional Group on Signal Processing and was the past Chairman of the IEEE UK&RI Signal Processing Chapter. He has also served on the technical committees of several International Conferences, and he was the Chairman of the first IEEE Signal Processing Systems Workshop in 1997.

Said Boussakta (S'86–M'90–SM'04) received the "Ingenieur d'Etat" degree in electronic engineering from Ecole Nationale Polytechnque of Algiers (ENPA), Algeria, in 1985 and the Ph.D. degree in electrical engineering (in signal and image processing) from the University of Newcastle-Upon-Tyne, U.K., in 1990.

From 1990 to 1996, he was working at the University of Newcastle-Upon-Tyne as a Senior Research Associate in digital signal and image processing. From 1996 to 2000, he was a Senior Lecturer in communications at the University of Teesside, U.K. He is currently a Reader in digital communications and signal processing at the School of Electronic and Electrical Engineering, University of Leeds, Leeds, U.K., where he is lecturing in modern communications networks, communications systems, and signal processing. He has authored and coauthored more than 100 publications. His research interests are in the areas of digital communications, security and cryptography, digital signal/image processing, and fast DSP algorithms and transforms.

Dr. Boussakta is a Senior Member of IEEE Signal Processing, Communications and Computer Societies and a Fellow of the Institution of Electrical Engineers (IEE).